IEEE Access
Multidisciplinary | Rapid Review | Open Access Journal

Received November 30, 2018, accepted December 19, 2018, date of publication January 1, 2019, date of current version April 5, 2019.

Digital Object Identifier 10.1109/ACCESS.2018.2890163

Comparative Study of Modular-Stator and Conventional Outer-Rotor Flux-Switching Permanent-Magnet Motors

JING ZHAO[1], (Member, IEEE), WENQI FU[1], YUN ZHENG[2], ZHEN CHEN[1], (Member, IEEE), AND YONGGUI WANG[1]

[1]School of Automation, Beijing Institute of Technology, Beijing 100081, China
[2]Department of Motor Power Supply, Beijing Aerospace Control Instrument Research Institute, Beijing 100085, China

Corresponding authors: Zhen Chen (chenzhen76@bit.edu.cn) and Yonggui Wang (wangyg1025@163.com)

This work was supported in part by the National Natural Science Foundation of China under Project 51677005, in part by the major project of Zhongshan city under Grant 2016A1027, and in part by the Intelligent Equipment and Technology of Automation Research and Development Platform under Grant 2016F2FC007.

ABSTRACT This paper presents the comparative studies of two permanent magnet (PM) motors, which are modular-stator outer-rotor flux-switching permanent-magnet (MSOR-FSPM) motor and conventional outer-rotor flux-switching permanent-magnet (COR-FSPM) motor. The differences in structure and design principles between the two types are compared. Then, a 2D finite element method (FEM) is used to analyze the basic electromagnetic performances. The magnetic field distribution, no-load back-EMF, cogging torque, and electromagnetic torque are presented and compared. Furthermore, a comprehensive comparison of the motor performances which are important for electric vehicles is investigated. The theoretical analysis and FEM results predict that the MSOR-FSPM motor has superior capability compared to that of the COR-FSPM motor, including fault tolerance capability, and field weakening capability.

INDEX TERMS Electric vehicles (EVs), flux-switching, permanent-magnet motor, modular-stator, outer-rotor.

I. INTRODUCTION

Electric vehicles (EVs) have attracted more and more attentions with the increased calling for environmental protection and energy conservation. Motors selected for EVs industry are expected to have high torque density, high power density and wide constant power speed range [1]. It creates an urgent demand for novel motors. With the advent of high-performance permanent-magnet (PM) material as well as the development of power electronics technology, novel topologies of stator PM brushless motors whose PMs are located on stator have been investigated in recent years. Especially, flux-switching permanent-magnet (FSPM) motor has been frequently researched for its high torque density and power density [2], [3]. The flux-linkage of FSPM motor is bipolar and the back-EMF can be designed to be sinusoidal. Compared with general PM motors, the FSPM motor has high field weakening capability, since the magnetic field excited by PMs is in parallel with that excited by armature currents [4]. In addition, the operating point of FSPM motor is more stable, and the fault tolerance capability is good [5]–[7]. Therefore, FSPM motors used for EVs attract more and more researches all over the world.

Besides, FSPM motor is also widely used in other fields. Axial FSPM motor that combines the characteristics of the conventional axial PM motor and FSPM motor, has short axial length and high power density, it has good prospects in the field of wind power generation [8]. Multi-phase FSPM motor has obvious advantages in low speed and high torque applications, such as reducing the rated torque of each phase, improving fault tolerance capability and control strategy flexibility, it is greatly introduced in high power and high reliability applications, such as aerospace and ship propulsion [9].

Outer-rotor FSPM motor, which combines the advantages of FSPM motor and outer-rotor motor, is generating more and more interest. Because it can be used as in-wheel motor in EVs industry to provide extra passenger space and independent direct control [10]. Moreover, it is convenient and low cost to maintain tires due to the simple rotor structure. The structure of an outer-rotor FSPM motor is first proposed in [11]. Many studies have been made to improve

its performances, including efficiency, field weakening capability, torque capability, and hybrid excitation [12]–[15]. However, the PM amount is too much and the coupling between three phases is obvious in these topologies proposed in references [11]–[15]. Therefore, a modular-stator outer-rotor flux-switching permanent-magnet (MSOR-FSPM) motor is proposed [16], whose PM amount is reduced by half, and the armature windings that belong to the same phase be concentrated in one stator module and non-magnetic blocks are purposely placed between the adjacent modules. Compared with conventional outer-rotor flux-switching permanent-magnet (COR-FSPM) motor, this kind of motor has good fault tolerant capability because modular stator structure reduces the interaction between the three phases, and the modular stator can be easily replaced.

In order to reasonably evaluate MSOR-FSPM motor, the different performances of MSOR-FSPM motor and COR-FSPM motor are compared in this paper. Firstly, the structure and design parameters of the two kind of motors are compared. Then the basic electromagnetic performances including magnetic field distribution, no-load back-EMF, cogging torque and electromagnetic torque are presented and compared by using the 2D finite element method (FEM). Next, considering the key performances of EVs, a comprehensive comparison on fault tolerance capability, field weakening capability, loss and efficiency is investigated. Finally, the performances of MSOR-FSPM motor are validated by experimental tests on the prototype motor.

II. STRUCTURE AND PARAMETERS OF THE 10POLE/12SLOT MSOR-FSPM MOTOR AND COR-FSPM MOTOR

A. STRUCTURE OF THE MSOR-FSPM MOTOR AND COR-FSPM MOTOR

The cross-sectional views of MSOR-FSPM motor and COR-FSPM motor are shown in Fig.1. Both of them are 10-pole/12-slot motors. The rotor of both motors consists of a simple laminated iron core with salient teeth. It can be seen from the cross-sectional view of MSOR-FSPM motor that the stator consists of three modules M_A, M_B, and M_C, which respectively represent the phase-A, phase-B and phase-C in the counter-clockwise direction. Non-magnetic material blocks are used between the adjacent modules. Each module consists of two ''V''-shaped laminated segments, one ''W''-shaped laminated segment, and two circumferential magnetized PMs with opposite polarity. The ''W''-shaped laminated segment is located in the middle of the module, ''V''-shaped laminated segments are located at the both ends of the module, and the PMs are sandwiched between the ''W''-shaped and ''V''-shaped laminated segments. The stator salient teeth wound with single-layer concentrated armature windings consist of ''W''-shaped and ''V''-shaped laminated segments. The stator of COR-FSPM motor consists of ''V''-shaped laminated segments and circumferential magnetized PMs with opposite polarity. Its stator salient teeth

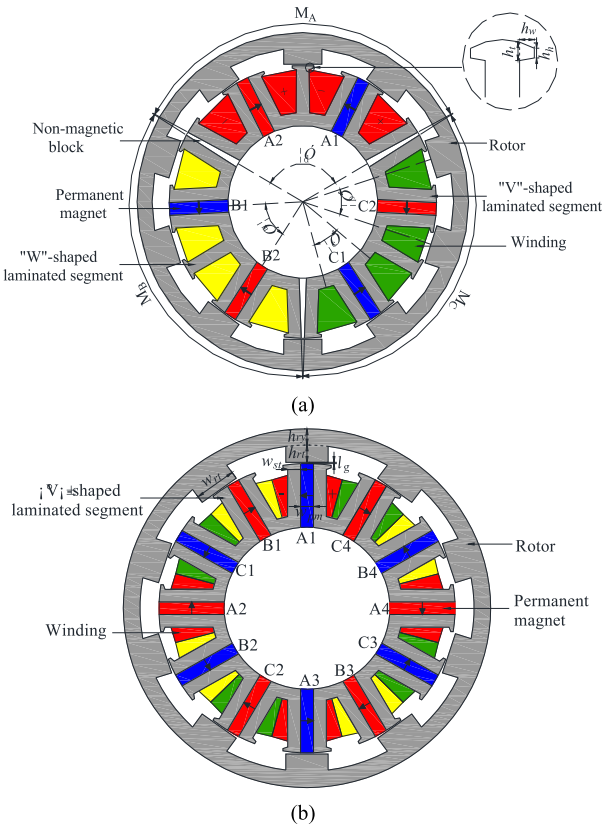

FIGURE 1. Cross-sectional view of (a) the MSOR-FSPM motor, and (b) the COR-FSPM motor.

wound with double-layer concentrated armature windings consist of ''V''-shaped laminated segments.

B. DESIGN PARAMETERS OF THE MSOR-FSPM MOTOR AND COR-FSPM MOTOR

The back-EMF period of the FSPM motor is one rotor pole pitch. Rotor pole pitch τ_p expressed as mechanical angle meets $\tau_p = 360°/N_r$, N_r is the number of rotor poles. In order to obtain good torque performance and balanced three-phase back-EMF, the main parameters of MSOR-FSPM motor should meet the following equations [17]:

$$\tau_c = h\tau_p \tag{1}$$

$$\tau_m = \left(i + 1/2^k\right)\tau_p \tag{2}$$

$$\tau_d = \left(j + 2^l/3\right)\tau_p \tag{3}$$

where the value of k and l is 0 or 1, i, j, and h are all non-negative integer, τ_c is the mechanical angle between the two adjacent slot conductors that belong to the same coil, τ_m is the mechanical angle between two adjacent PMs in each module, τ_d is the mechanical angle between two adjacent modules.

Equation (1) and equation (2) can make the winding factor close to 1. Equation (3) can make the phase difference of back-EMF between different windings be 120° (electrical angle).

The design of other dimensions in MSOR-FSPM motor can reference COR-FSPM motor [11]–[14]. In order to fairly

TABLE 1. Dimensions Of Msor-Fspm motor and Cor-Fspm motor.

Symbol	Machine Parameters	MSOR-FSPM-1	MSOR-FSPM-2	COR-FSPM
n	Base speed (r/min)	800	800	800
D_{ro}	Rotor outer diameter (mm)	155	155	155
D_{si}	Stator inner diameter (mm)	70	70	70
D_{so}	Stator outer diameter (mm)	125	125	125
l_{ef}	Motor active length (mm)	100	100	100
h_{rt}	Rotor tooth height (mm)	7.5	7.5	7.5
h_{ry}	Rotor yoke height (mm)	7	7	7
w_{rt}	Rotor tooth width (mm)	17.78	17.78	17.78
l_g	Air-gap length (mm)	0.5	0.5	0.5
B_r	Magnet remanence (T)	1.26	1.26	1.26
h_t	Pole shoe thickness (mm)	2	2	2
h_w	Pole shoe width (mm)	2	2	2
h_h	Pole shoe height (mm)	1	1	1
I_{smax}	Rated current amplitude (A)	15.4	15.4	15.4
w_{st}	Stator tooth width (mm)	5.50	5.50	5.50
N_{coil}	Number of turns per coil	70	81	35
S_{slot}	Area per phase (mm2)	955.44	955.44	785.28
V_{pm}	Volume of PMs (mm3)	97185	97185	179850

compare the performances, the main parameters and current density of both motors are the same. The design dimensions of MSOR-FSPM motor and COR-FSPM motor are illustrated in Fig.1 and listed in Table 1. The performances at no-load is not effected by the windings. However, when the motors operate at load, the winding parameter is important. In table 1, MSOR-FSPM-1 motor has the same number of turns per phase with COR-FSPM motor. Actually, the slot area per phase of the MSOR-FSPM motor is enlarged because of the reduction of PMs, and its stator slot fill factor is smaller than that of the COR-FSPM motor. Thus, parameters of MSOR-FSPM-2 motor, which has the same stator slot fill factor with COR-FSPM motor, is also given.

III. BASIC ELECTROMAGNETIC PERFORMANCES OF MSOR-FSPM MOTOR AND COR-FSPM MOTOR

A. MAGNETIC FIELD DISTRIBUTION

The no-load magnetic field distributions of MSOR-FSPM motor and COR-FSPM motor are shown in Fig.2 (a). For both motors, the magnetic lines are more intensive and the magnetic density is larger when the stator teeth are closer to the air gap. However, in COR-FSPM motor, the magnetic density in stator yoke is smaller than that in stator teeth, while, in MSOR-FSPM motor, the magnetic density of certain stator yoke is quite close to that of the stator teeth. In addition, the magnetic density of rotor yoke in MSOR-FSPM motor is generally higher than that of COR-FSPM motor.

The radial air-gap magnetic flux density in MSOR-FSPM motor and COR-FSPM motor are shown in Fig.2 (b). In MSOR-FSPM motor, the air-gap magnetic flux density is larger than that of general PM motors due to the assembled magnetic effect, which is similar to COR-FSPM motor. The amplitude of radial magnetic density in air gap can be as high as 2T, which indicates the torque capacity of MSOR-FSPM motor is larger than that of general PM motors [18].

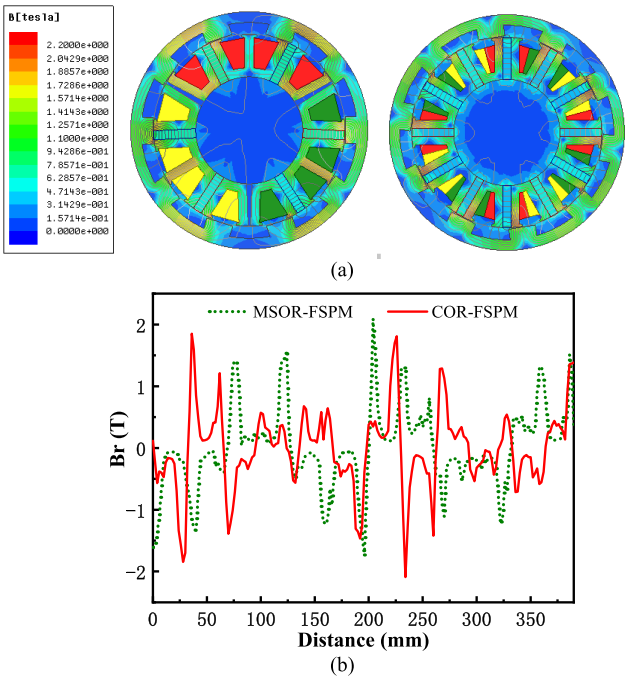

FIGURE 2. (a) No-load magnetic field distributions of MSOR-FSPM motor and COR-FSPM motor. (b) Air-gap radial magnetic density of MSOR-FSPM motor and COR-FSPM motor.

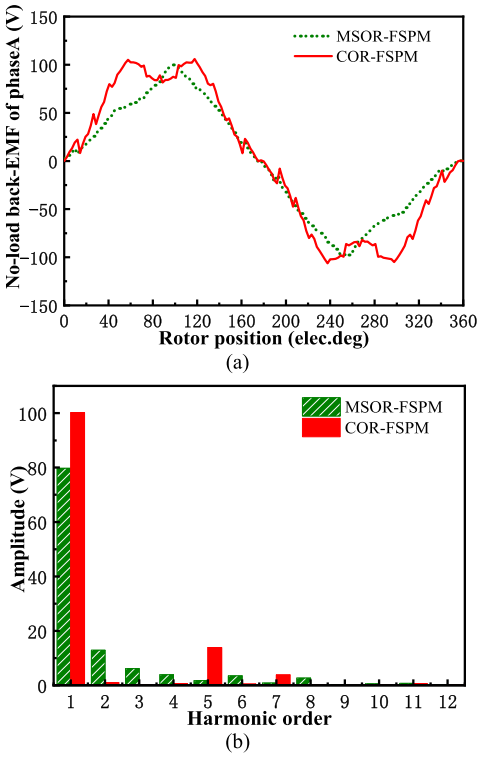

FIGURE 3. (a) No-load back-EMF waveforms of MSOR-FSPM motor and COR-FSPM motor. (b) Harmonic analysis of no-load back-EMF in MSOR-FSPM motor and COR-FSPM motor.

B. NO-LOAD BACK-EMF

The no-load back-EMF waveforms of the two motors are shown in Fig.3 (a) and the harmonic analysis results of them are shown in Fig.3 (b). It can be seen that the distortion

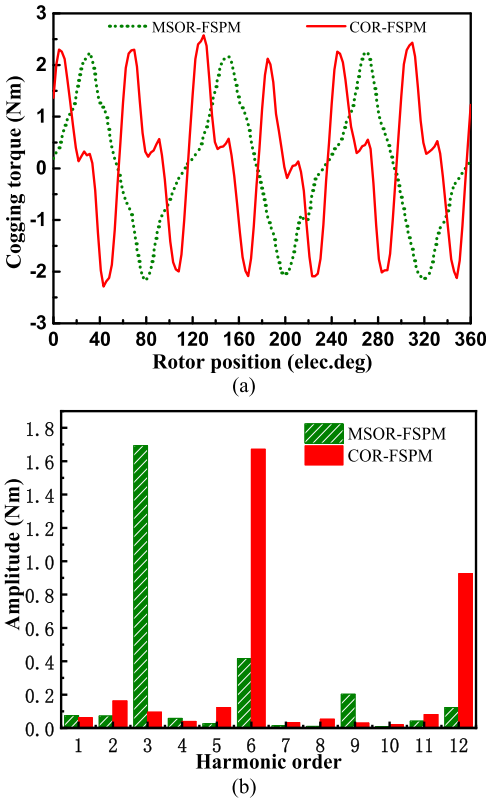

FIGURE 4. (a) Cogging torque waveforms of MSOR-FSPM motor and COR-FSPM motor. (b) Harmonic analysis of cogging torque in MSOR-FSPM motor and COR-FSPM motor.

of waveforms is serious. In addition to the fundamental wave, the no-load back-EMF of MSOR-FSPM motor mainly contains the 2nd, 3rd, 4th, 6th, and 8th harmonics. But for the COR-FSPM motor, besides the fundamental wave, the no-load back-EMF mainly contains the 5th and 7th harmonics. Total harmonic distortions (THD) of no-load back-EMF in MSOR-FSPM motor and COR-FSPM motor are 19.57% and 14.46%, respectively. Besides the cogging torque, when sinusoidal current is fed into windings, the distortion of no-load back-EMF can also lead to torque harmonics, which will affect the stability of the motor.

C. COGGING TORQUE

In the general FSPM motor, the electrical period of cogging torque meets the following equations [19]:

$$N_p = N_r / HCF\{N_s, N_r\} \tag{4}$$

$$\theta_{cog.elec} = 360^\circ N_r / (N_p \cdot N_s) \tag{5}$$

where N_s is the number of stator slots, $HCF\{\}$ is the greatest common divisor of N_r and N_s, N_p is a coefficient depended on the number of slots and poles.

For the COR-FSPM motor with $N_r = 10$, $N_s = 12$, the electrical period of cogging torque is 60°. The cogging torque waveforms of both motors are shown in Fig.4 (a). The 2D FEM results show that the electrical period of cogging torque in COR-FSPM motor is completely consistent with the theoretical analysis. However, the electrical period of

TABLE 2. Harmonic analysis of cogging torque for each stator module.

Harmonic	M_A (Nm)	M_B (Nm)	M_C (Nm)	Degree AB (°)	Degree BC (°)	Degree CA (°)
1st	4.01	4.14	4.28	119.65	122.05	118.29
2nd	1.72	1.58	1.57	121.91	114.70	123.38
3rd	0.48	0.60	0.56	2.57	10.28	7.71
4th	1.38	1.34	1.35	119.48	120.78	119.74
5th	0.70	0.70	0.71	115.70	127.99	116.30
6th	0.16	0.23	0.23	18.13	17.46	0.67
7th	0.08	0.04	0.03	174.74	55.51	129.76
8th	0.22	0.18	0.19	123.02	119.55	117.42
9th	0.07	0.07	0.07	5.58	2.36	7.94

cogging torque in MSOR-FSPM motor no longer meets the above equations, and it is two times that of COR-FSPM motor. This is the result of the vector synthesis of the cogging torque harmonics among three stator modules. The harmonic analysis results of cogging torque for each module are listed in Table 2. It can be seen that for the 1st, 2nd, 4th, 5th, 8th harmonics, amplitude of the same harmonic is approximately equal to each other and the phase difference of the same harmonic between the two adjacent modules is approximately equal to 120° (electrical angle). Furthermore, the synthetic vector of the 7th harmonic in module B and module C is approximately equal to the amplitude of the 7th harmonic in module A and the phase difference is approximately equal to 180° (electrical angle). Therefore the amplitude of the 1st, 2nd, 4th, 5th, 7th and 8th harmonics in stator is small. For the 3rd, 6th and 9th harmonics, amplitude and the phase difference of the same harmonic between the two adjacent modules are approximately equal to each other. Therefore the amplitude of the 3rd, 6th and 9th harmonics in stator is large. The harmonic analysis results of cogging torque in both motors are shown in Fig.4 (b). MSOR-FSPM motor mainly contains the 3rd, 6th, 9th, and 12th harmonics, especially the 3rd harmonic. COR-FSPM motor mainly contains the 6th and 12th harmonics.

D. ELECTROMAGNETIC TORQUE

When the motors operate at load, the winding parameter effects the motor performance. Thus, MSOR-FSPM-1 motor, MSOR-FSPM-2 motor and COR-FSPM motor are compared at following research.

Motors adopt $I_d = 0$ vector control, sinusoidal current whose amplitude is 15.4A is fed into windings, and the electromagnetic torque waveforms are shown in Fig.5.

The average torque of MSOR-FSPM-1 motor and COR-FSPM motor is 20.97Nm and 27.61Nm, respectively. Although the PM volume of MSOR-FSPM-1 motor is 54.04% of that in COR-FSPM motor, its average torque is 75.95% of that in COR-FSPM motor. The utilization of PM in MSOR-FSPM-1 motor is higher than that of COR-FSPM motor. However, this comparison is based on the same number of turns per phase. When the stator slot fill factor of MSOR-FSPM motor is the same with COR-FSPM motor, the average electromagnetic torque in MSOR-FSPM-2 motor

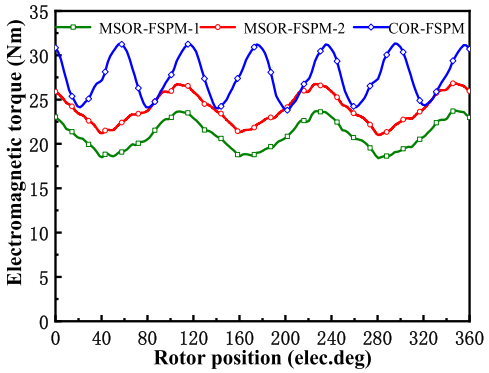

FIGURE 5. Electromagnetic torque waveforms of MSOR-FSPM motor and COR-FSPM motor.

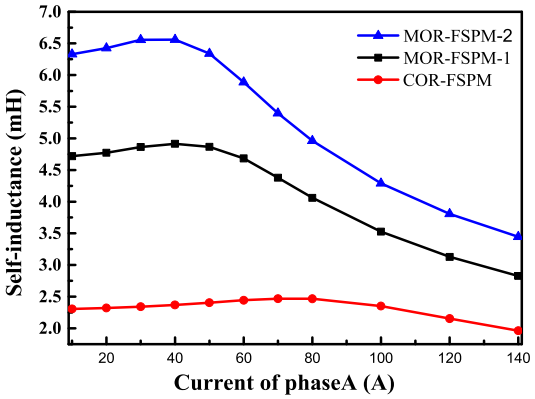

FIGURE 6. Self-inductance of MSOR-FSPM motor and COR-FSPM motor with increasing current.

is 23.98Nm, and the utilization of PM is further improved, with about half PMs but providing 86.53% average torque compared to the COR-FSPM motor.

IV. MAIN PERFORMANCES USED FOR EVS

A. FAULT TOLERANCE CAPABILITY

Fault tolerance capability is an important feature for the motor used for EVs. It needs the remaining two-phase windings can continue to work when malfunction occurs in one phase, which requires the motor has a low mutual-inductance. Thus, the fault tolerance capability of the two motors are evaluated by inductances. In order to reduce short-circuit current of the motor, it is necessary to increase the self-inductance of each phase as much as possible [20], [11].

Taking phase A as an example, DC current is fed into this windings, the current of other two phases is equal to zero, self-inductance and mutual-inductance can be obtained by the following equations:

$$\psi_a = L_{aa} i_a + \psi_{m\_a} = \Lambda_a N_{coil}^2 \tag{6}$$

$$L_{aa} = \left(\psi_a - \psi_{m\_a}\right)/i_a \tag{7}$$

$$L_{ab} = \left(\psi_b - \psi_{m\_b}\right)/i_a \tag{8}$$

$$L_{ac} = \left(\psi_c - \psi_{m\_c}\right)/i_a \tag{9}$$

where Ψ_a is the total flux linkage of phase A; L_{aa} is the self-inductance of phase A, L_{ab} is the mutual-inductance of phase A and phase B, L_{ac} is the mutual-inductance of phase A and phase C;i_a is the current of phase A; Ψ_{m_a}, Ψ_{m_b} and Ψ_{m_c} are the PM flux linkage of phase A, phase B and phase C, respectively; Λ_a is the permeability of magnetic circuit in phase A.

Obviously, the self-inductance is not only related to the number of coil turns, but also to the permeability of magnetic circuit. The permeability of magnetic circuit is affected by the saturation caused by the PMs and armature current. The variation of self-inductance with increasing current is shown in Fig.6. Self-inductances of MSOR-FSPM-1 motor and MSOR-FSPM-2 motor have similar change trend. When the armature current is less than 40A, the self-inductance changes little. When the armature current is larger than 40A, the magnetic circuit reaches supersaturated state and self-inductance is reduced. The self-inductance trend of COR-FSPM motor is similar to that of MSOR-FSPM motor, but the armature current that makes magnetic circuit reach supersaturated state is 80A. It can be found that MSOR-FSPM motor is more likely to reach the supersaturated state, and self-inductance is reduced sharply with the increasing armature current after motor reaching the supersaturated state.

TABLE 3. Inductance comparisons Of Msor-Fspm motor and Cor-Fspm motor.

Parameters	MSOR-FSPM-1	MSOR-FSPM-2	COR-FSPM
Self-inductance (mH)	4.74	6.36	2.31
Mutual-inductance (mH)	0.43	0.57	1.11

The self-inductances and mutual-inductances of the MSOR-FSPM-1 motor, MSOR-FSPM-2 motor and the COR-FSPM motor are obtained by FEM and shown in Table 3. As is seen from Table 3, the average self-inductance value is equal to two times that of mutual-inductance in COR-FSPM motor. The verage value of self-inductance is far more than two times that of mutual-inductance in MSOR-FSPM-1 motor. In addition, self-inductance of MSOR-FSPM-1 motor is larger than two times that of COR-FSPM motor, and mutual-inductance is smaller than half that of COR-FSPM motor. However, the comparison between MSOR-FSPM-1 motor and COR-FSPM motor is based on the same number of turns per phase. When the stator slot fill factor of MSOR-FSPM-2 motor is the same with COR-FSPM motor, the self-inductance of MSOR-FSPM motor is further enlarged to 6.36mH and the mutual-inductance is still smaller than that of COR-FSPM motor. Therefore, the fault tolerance capability of outer-rotor FSPM motor is improved after stator is modularized.

B. FIELD WEAKENING CAPABILITY

Motor runs in the constant torque region before reaching the rated speed. With the speed increasing, the back-EMF increases. When back-EMF is higher than the voltage provided by the DC bus, the inverter cannot provide energy to the motor. In order to make the motor run at higher speed, it can adjust the phase angle of armature current and increase

the d-axis demagnetization current to keep the voltage balanced. When the d-axis current research the limit current, the armature current fully produces demagnetization flux and the motor reaches the maximum speed, which satisfies the following equation [11]:

$$\omega_{\max} = U_{\max}/N_r\,(\psi_m - L_d I_{\max}) \tag{10}$$

where $U_{\max}$ is the maximum voltage provided by the DC bus; Ψ_m is the flux linkage produced by PMs; L_d is the inductance of d-axis; $I_{\max}$ is the peak value of the rated phase current.

In order to quantify the field weakening capability, flux weakening coefficient K_{fw} and speed extension ratio β can be calculated as follows, respectively [11]:

$$K_{fw} = \psi_d/\psi_m = L_d I_{\max}/\psi_m \tag{11}$$

$$\beta = 1/(1 - K_{fw}) \tag{12}$$

When K_{fw} is less than 1, the flux linkage produced by PMs cannot be fully weakened by demagnetization flux produced by d-axis current, the motor can only work in the limited speed range; when K_{fw} is greater than 1, the flux linkage produced by PMs can be fully weakened by demagnetization flux produced by d-axis current, theoretical speed range can reach infinity.

The electromagnetic torque in the field weakening mode is [12]:

$$T_{em} = 3N_r\left[2\psi_m I_{\max}\cos\varphi - (L_d - L_q)\,I_{\max}^2\sin\,2\varphi\right]/4 \tag{13}$$

where φ is the phase angle between current vector and rotor q-axis; L_q is the inductance of q-axis.

TABLE 4. Field weakening capability In Msor-Fspm motor and Cor-Fspm motor.

Parameters	MSOR-FSPM-1	MSOR-FSPM-2	COR-FSPM
Ψ_m (Wb)	0.09586	0.11092	0.12039
L_d (mH)	4.78	6.23	2.82
L_q (mH)	5.61	7.81	3.55
K_{fw}	0.77	0.86	0.36
β	4.31	7.14	1.56

When the maximum demagnetization current is fed into windings, the field weakening capability of MSOR-FSPM motor and COR-FSPM motor are shown in Table 4. It can be found that the flux linkage produced by PMs of MSOR-FSPM-1 is 79.62% of that in COR-FSPM motor when the number of turns per phase is the same, and the flux linkage produced by PMs of MSOR-FSPM-2 is 92.13% of that in COR-FSPM motor when the stator slot fill factor is the same. Moreover, L_d is less than L_q in MSOR-FSPM motor and COR-FSPM motor, reluctance torque is conducive to increase the electromagnetic torque during field weakening operation.

It is worth noting that the flux weakening coefficient K_{fw} of MSOR-FSPM motor is much larger than that of COR-FSPM motor. The speed extension ratio β of MSOR-FSPM motor is 2.76 times that of COR-FSPM motor when the number of turns per phase in motors is the same, and it is enlarged to 4.58 times that of COR-FSPM motor when the stator slot fill factor of motors is the same. Therefore, the field weakening capability of MSOR-FSPM motor is better than that of COR-FSPM motor.

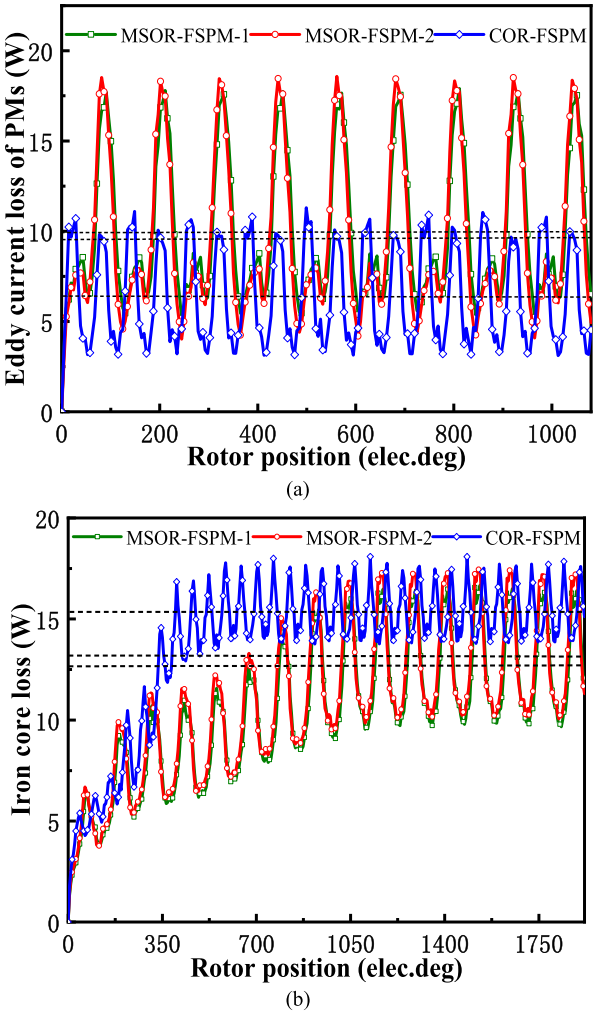

FIGURE 7. (a) PMs eddy current loss waveforms with different rotor position at rated operating state. (b). Iron core loss waveforms with different rotor position at rated operating state.

C. LOSS AND EFFICIENCY

1) RATED OPERATING STATE

At the rated current and rated speed operating condition, the copper losses of windings in MSOR-FSPM-1 motor, MSOR-FSPM-2 motor and COR-FSPM motor are 115.93W, 134.15W and 112.41W, respectively. The PMs eddy current loss and iron core loss in three motors are shown in Fig.7. The period of PMs eddy current loss and iron core loss in MSOR-FSPM motor is two times that of COR-FSPM motor, because the PMs circumferential distance and the magnetic density period of MSOR-FSPM motor are about two times that of COR-FSPM motor. The PMs eddy current losses of MSOR-FSPM-1 motor, MSOR-FSPM-2 motor, and COR-FSPM motor are 9.96W, 9.68W and 6.38W, respectively.

The iron core losses of MSOR-FSPM-1 motor, MSOR-FSPM-2 motor and COR-FSPM motor are 12.71W, 13.17W, and 15.35W, respectively. If the wind friction loss and other loss are ignored, the efficiency of MSOR-FSPM-1 motor, MSOR-FSPM-2 motor and COR-FSPM motor is 92.68%, 92.71%, and 94.52%, respectively. The efficiency of MSOR-FSPM motor is slightly smaller than that of COR-FSPM motor, but it is still the high efficiency PM motor compared with other type motors.

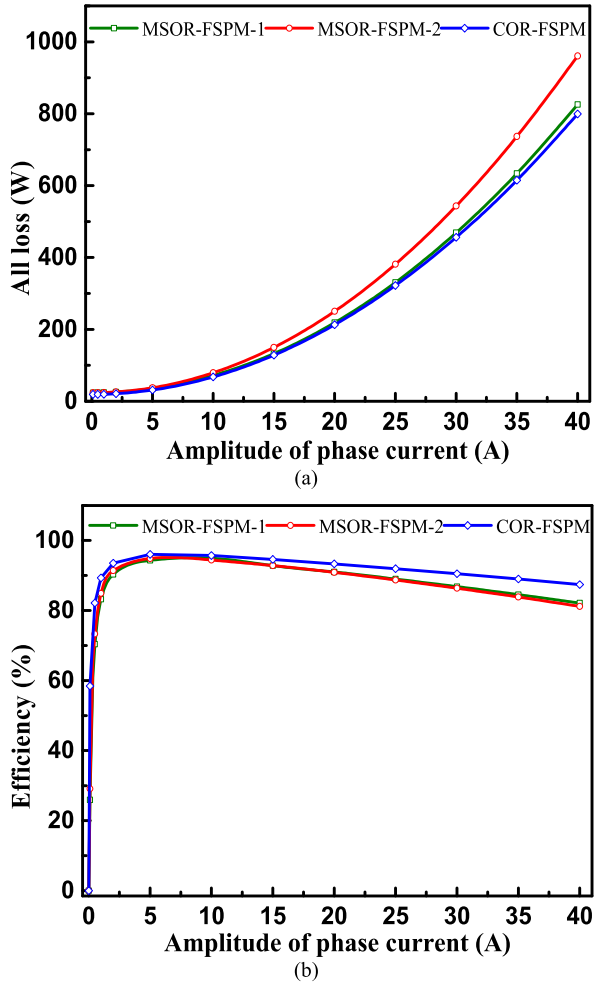

FIGURE 8. Loss and efficiency (a). Total loss with increasing current. (b) Efficiency with increasing current.

2) DIFFERENT CURRENT

The speed of motor is kept the rated value and the amplitude of phase current is changed. The variation of total loss, including eddy current loss of PMs, iron core loss and copper loss, is shown in Fig.8 (a). When the number of turns per phase is the same, the total losses of MSOR-FSPM motor and COR-FSPM motor are almost equal to each other, and are sharply enlarged with increasing current. When the stator slot fill factor is the same and phase current is smaller than 10A, the total losses of MSOR-FSPM motor and COR-FSPM motor are also almost equal to each other. When the stator slot fill factor is the same and phase current is larger than 10A, the total loss of MSOR-FSPM motor is larger than that of COR-FSPM motor, because with increasing current, the variation of copper loss in MSOR-FSPM motor is much larger than that of COR-FSPM.

The variation of efficiency in three motors is shown in Fig.8 (b). The copper loss is unremarkable when the current is small, the electromagnetic power is enlarged with the increasing current and the efficiency increases at first. With current continuous increasing, the copper loss is increased significantly, the efficiency then decreases. It can be found that the efficiency of MSOR-FSPM motor is lower than that of COR-FSPM motor.

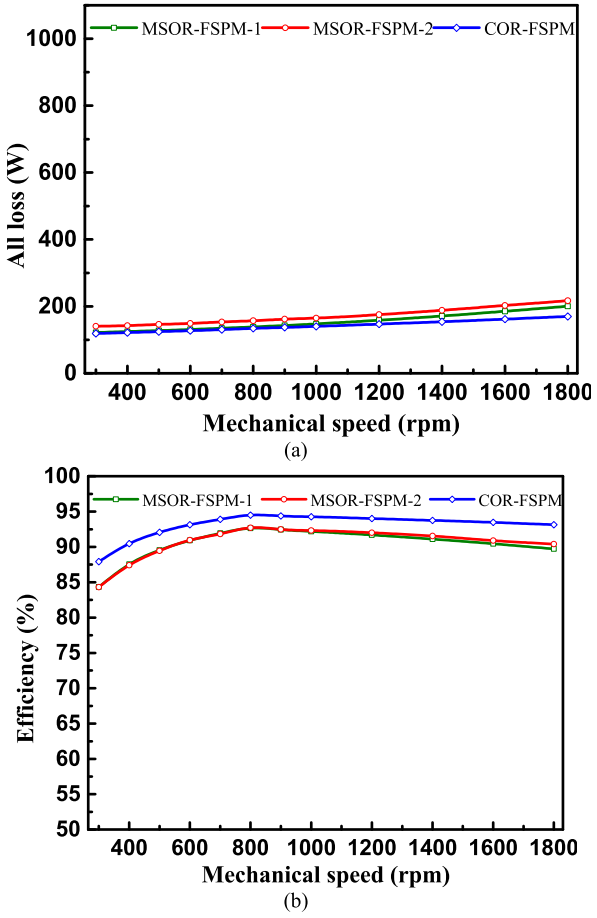

FIGURE 9. (a) Total loss with increasing mechanical speed at rated load current. (b) Efficiency with increasing mechanical speed at rated load current.

3) DIFFERENT SPEED

When the current of motor is kept the rated value, variation of total loss with increasing mechanical speed is shown in Fig.9 (a). The total loss of MSOR-FSPM-2 motor is larger than that of the other two motors, due to the larger copper loss. When the speed is smaller than 900rpm, the total loss of MOR-FSPM-1 motor and COR-FSPM motor is equal to each other. When the speed is larger than 900rpm, the total loss of MOR-FSPM-1 motor is bigger than that of COR-FSPM motor, and the difference between them becomes larger and larger with the increasing mechanical speed. The variation of

efficiency in three motors is shown in Fig.9 (b). Efficiency of MSOR-FSPM motor is smaller than that of COR-FSPM motor. The efficiency of three motors is firstly increased and then decreased with increasing mechanical speed, reaching the maximum value at the rated speed.

In general, no matter what operating state is, the total loss of MSOR-FSPM motor is larger than that of COR-FSPM motor and the efficiency of MSOR-FSPM motor is slightly smaller than that of COR-FSPM motor.

V. CONCLUSION

In this paper, the performances of MSOR-FSPM motor and COR-FSPM motor are compared. The electrical period of cogging torque in MSOR-FSPM motor no longer meets the conventional formula. The utilization of PM in MSOR-FSPM motor is higher than that of COR-FSPM motor, which is verified by the results of FEM. The self-inductance is enlarged and mutual-inductance is reduced when the modular stator structure is adopted, which improves the fault tolerance capability of MSOR-FSPM motor. Moreover, the field weakening capability of MSOR-FSPM motor is better than that of COR-FSPM motor. In addition, the loss of MSOR-FSPM motor is slightly larger than that of COR-FSPM motor and the efficiency of MSOR-FSPM motor is slightly smaller than that of COR-FSPM motor, but it still belongs to the high efficiency PM motor. In general, MSOR-FSPM motor has superior capability to that of COR-FSPM motor when it is used in EVs.

REFERENCES

[1] E. A. Lomonova, E. Kazmin, Y. Tang, and J. J. H. Paulides, "In-wheel PM motor: Compromise between high power density and extended speed capability," *Int. J. Comput. Math. Elect. Electron. Eng.*, vol. 30, no. 1, pp. 98–116, 2011.

[2] Y. Shi, L. Jian, J. Wei, Z. Shao, W. Li, and C. C. Chan, "A new perspective on the operating principle of flux-switching permanent-magnet machines," *IEEE Trans. Ind. Electron.*, vol. 63, no. 3, pp. 1425–1437, Mar. 2016.

[3] A. R. Salisa, N. Zhang, and J. G. Zhu, "A comparative analysis of fuel economy and emissions between a conventional HEV and the UTS PHEV," *IEEE Trans. Veh. Technol.*, vol. 60, no. 1, pp. 44–54, Jan. 2011.

[4] A. S. Thomas, Z. Q. Zhu, and G. W. Jewell, "Proximity loss study in high speed flux-switching permanent magnet machine," *IEEE Trans. Magn.*, vol. 45, no. 10, pp. 4748–4751, Oct. 2009.

[5] K. T. Chau, C. C. Chan, and C. Liu, "Overview of permanent-magnet brushless drives for electric and hybrid electric vehicles," *IEEE Trans. Ind. Electron.*, vol. 55, no. 6, pp. 2246–2257, Jun. 2008.

[6] Z. Q. Zhu and D. Howe, "Electrical machines and drives for electric, hybrid, and fuel cell vehicles," *Proc. IEEE*, vol. 95, no. 4, pp. 746–765, Apr. 2007.

[7] W. Hua, M. Cheng, H. Jia, and X. Fu, "Comparative study of flux-switching and doubly-salient PM machines particularly on torque capability," in *Proc. IEEE Ind. Appl. Soc. Annu. Meeting*, Oct. 2008, pp. 1–8.

[8] L. Shao, W. Hua, N. Dai, M. Tong, and M. Cheng, "Mathematical modeling of a 12-phase flux-switching permanent-magnet machine for wind power generation," *IEEE Trans. Ind. Electron.*, vol. 63, no. 1, pp. 504–516, Jan. 2016.

[9] F. Li, W. Hua, M. Tong, G. Zhao, and M. Cheng, "Nine-phase flux-switching permanent magnet brushless machine for low-speed and high-torque applications," *IEEE Trans. Magn.*, vol. 51, no. 3, Mar. 2015, Art. no. 8700204.

[10] M. Ehsani, Y. Gao, and J. M. Miller, "Hybrid electric vehicles: Architecture and motor drives," *Proc. IEEE*, vol. 95, no. 4, pp. 719–728, Apr. 2007.

[11] Y. Wang, M.-J. Jin, J.-X. Shen, W. Z. Fei, and P. C. K. Luk, "An outer-rotor flux-switching permanent magnet machine for traction applications," in *Proc. IEEE Energy Convers. Congr. Expo. (ECCE)*, Sep. 2010, pp. 1723–1730.

[12] W. Fei, P. C. K. Luk, J. X. Shen, Y. Wang, and M. Jin, "A novel permanent-magnet flux switching machine with an outer-rotor configuration for in-wheel light traction applications," *IEEE Trans. Ind. Appl.*, vol. 48, no. 5, pp. 1496–1506, Sep./Oct. 2012.

[13] W. Hua, H. L. Zhang, M. Cheng, J. Meng, and C. Hou, "An outer-rotor flux-switching permanent-magnet-machine with wedge-shaped magnets for in-wheel light traction," *IEEE Trans. Ind. Electron.*, vol. 64, no. 1, pp. 69–80, Jan. 2017.

[14] X. Zhu, Z. Shu, L. Quan, Z. Xiang, and X. Pan, "Multi-objective optimization of an outer-rotor V-shaped permanent magnet flux switching motor based on multi-level design method," *IEEE Trans. Magn.*, vol. 52, no. 10, Oct. 2016, Art. no. 8205508.

[15] M. Z. Ahmad, E. Sulaiman, Z. A. Haron, and T. Kosaka, "Preliminary studies on a new outer-rotor permanent magnet flux switching machine with hybrid excitation flux for direct drive EV applications," in *Proc. IEEE Int. Conf. Power Energy*, vol. 48, no. 11, Dec. 2012, pp. 928–933.

[16] J. Zhao, Y. Zheng, C. Zhu, X. Liu, and B. Li, "A novel modular-stator outer-rotor flux-switching permanent-magnet motor," *Energies*, vol. 10, no. 7, Jul. 2017, Art. no. 937.

[17] X. Liu, Z. Gu, and J. Zhao, "Torque ripple reduction of a novel modular arc-linear flux-switching permanent-magnet motor with rotor step skewing," *Energies*, vol. 9, no. 6, May 2016, Art. no. 404.

[18] W. Hua, M. Cheng, Z. Q. Zhu, and D. Howe, "Analysis and optimization of back EMF waveform of a flux-switching permanent magnet motor," *IEEE Trans. Energy Convers.*, vol. 23, no. 3, pp. 727–733, Sep. 2008.

[19] N. Bianchi and S. Bolognani, "Design techniques for reducing the cogging torque in surface-mounted PM motors," *IEEE Trans. Ind. Appl.*, vol. 38, no. 5, pp. 1259–1265, Sep./Oct. 2002.

[20] H. J. P. Johannes and J. K. Maarten, "Design of new concept direct grid-connected slip-synchronous permanent-magnet wind generator," *IEEE Trans. Ind. Appl.*, vol. 48, no. 3, pp. 913–922, May/Jun. 2012.

JING ZHAO (M'13) received the B.Sc. degree from the Hebei University of Technology, Tianjin, China, in 2005, and the M.Sc. and Ph.D. degrees from the Harbin Institute of Technology, Harbin, China, in 2007 and 2011, respectively, all in electrical engineering.

She is currently an Associate Professor with the School of Automation, Beijing Institute of Technology, Beijing, China. Her research interests include electric machines and drive systems used for renewable energy and special servo machines systems.

WENQI FU received the B.E. degree in automation from the North China University of Technology, Beijing, China, in 2018. She is currently pursuing the M.Sc. degree with the School of Automation, Beijing Institute of Technology, Beijing.

Her research interests include modeling and design of PM machines and new permanent magnet motor systems.

YUN ZHENG received the B.E. and M.Sc. degrees from the Beijing Institute of Technology, Beijing, China, in 2015 and 2018, respectively.

She is currently working at the Beijing Aerospace Control Instrument Research Institute, Beijing. Her research interests include torque motor for inertial platform systems and permanent magnet motors.

ZHEN CHEN (M'11) received the B.Sc. degree from Northeast Petroleum University, Daqing, China, in 1999, and the M.Sc. and Ph.D. degrees from the Beijing Institute of Technology, Beijing, China, in 2005 and 2008, respectively.

He is currently an Associate Professor, a Doctoral Supervisor, and a Master Tutor with the School of Automation, Beijing Institute of Technology, Beijing. His research interests include the research work of spacecraft attitude control, high precision servo systems, nonlinear system control theory, and motor drive control direction.

YONGGUI WANG received the B.E. degree from the Qingdao University of Science and Technology, in 2011, and the Ph.D. degree from the Beijing Institute of Technology, Beijing, China, in 2017, all in mechanical engineering.

He held a Postdoctoral position at the School of Mechatronical Engineering, Beijing Institute of Technology, since 2015. His research interests include control systems of surgical robots and image recognition.